Int. J. Electrochem. Sci., 17 **(2022)** Article Number: 22085, doi: 10.20964/2022.08.09

International Journal of
ELECTROCHEMICAL
SCIENCE
www.electrochemsci.org

Short Communication

Preparation of lignin-derived carbon/sulfur composites and their lithium storage properties

Haojie Li, Leiting Han, Ruhua Jing, Zeren Liu, Sijing Chen, Bo Zhang, Tanan Yu, Wei Yan, Liping Wan, Jinkai Yao, Chengsai Xu, Hanning Guo, Chen Tai, Yutao Zhang and Zhengping Zhao[*]

Zhijiang College, Zhejiang University of Technology, Hangzhou 310014, P.R. China
[*]E-mail: sjzhaolei@163.com

Received: 5 December 2021 / *Accepted:* 12 March 2022 / *Published:* 4 July 2022

A large amount of lignin in waste liquid of agricultural straw and paper industry cannot be effectively utilized. Porous carbon materials have the advantages of stable chemical and thermal properties and easy processing, and have a wide application prospect in supercapacitor electrode, solid hydrogen storage and other fields. In this paper, lignin-based carbon spheres were prepared by ultrasonic self-assembly and high-temperature calcination. The lignin-based C/S composite microspheres were formed by loading sulfur with supercritical carbon dioxide method. The surface of lignin carbon spheres is rich in mesoporous and has a high degree of graphitization, and sulfur elements are uniformly loaded on the surface of the microspheres. Then, the lignin-based C/S composite electrode was prepared and electrochemical test was carried out. The results showed that the first discharge capacity of the lignin-based C/S composite electrode was 1172 $mAh \cdot g^{-1}$ at the current density of 0.1 $mAh \cdot g^{-1}$, and the capacity remained at 570 $mAh \cdot g^{-1}$ after 1100 charge and discharge cycles, and the capacity retention rate was 48.6%.

Keywords: lignin, mesoporous carbon, hydro-thermal synthesis, electrochemistry performance

1. INTRODUCTION

Lithium ion anode material is carbon and its composite material, in which the porous carbon with large specific surface area is the main material [1]. Porous carbon can be prepared by template method, direct carbonization method and activation method. Template method can be divided into soft template method and hard template method [2]. Soft template method requires a template for self-assembly of polymer materials as the carbon source, such as supramolecular, amphiphilic polymer, etc. In addition, self-supporting space-oriented materials can be used to construct pore structures. For example, ordered structures can be formed by intermolecular hydrogen bonding and other intermolecular forces, and then ordered porous carbon materials can be obtained through carbonization [3]. The hard template method

takes hard inorganic porous materials as the base, introduces the organic polymer carbon source into the gap of the template, carbonizes at high temperature and washes away the template to obtain porous carbon materials [4]. Sterk synthesized mesoporous carbon materials in the presence of ethyl orthosilicate (TEOS) using triblock copolymer F127 and phenolic resin as precursors with BET area up to 780 $m^2 \cdot g^{-1}$ [5]. Direct carbonization, which breaks down the organic material at high temperature, leaving the carbon shelf. This method is simple and direct, but has high requirements on organic precursors, which are mainly including polymers, biological materials and ionic liquids [6]. Activation is a physical or chemical method to directly improve the internal pore size or number of holes in a carbon material. Physical activation method is mainly the first precursor carbonization, and then add activator, activation at a higher temperature, part of the components of the gasification of the internal action of the material to produce pores. The chemical activation method requires the mixture of activator and precursor to be heated to a high enough temperature to complete the activation during carbonization [7]. Van de Pas used pre-chemically treated lignin to react with fungal laccase and change the surface properties of lignin through polymerization [8]. Fiddler reported that the phenylpropane side chain of lignin degrades in the temperature range of 230~260℃ to form methyl, ethyl and vinyl guaiacol and vanillin [9]. The β-β and C-C bonds between the units were cleaved at 275-350℃, which leading to free radical recombination to produce guaiac-based and syringyl compounds. Wu studied the lignin oxidation using CuO as a substitute for nitrobenzene and obtained 7-8% aldehydes [10]. Goheen obtained phenol by reducing lignin with sulfide metal catalyst [11]. But lignin itself also has a number of attractive properties that have stimulated researchers' interest in developing lignin into a variety of higher value-added products.

Although the carbon-sulfur composite material of lithium-sulfur battery has the characteristics of high energy density and high specific capacity, the defects of the electrode itself, such as the non-metallic insulating properties of sulfur and its electrochemical products. The soluble sulfide produced in the electrochemical process of the battery, restrict the subsequent cyclic reactions. In addition, these shortcomings also cause problems such as low utilization rate of active substances, short cycle life and fast capacity attenuation of the system [12-14]. The reasons for these problems are as follows: bulk strain of sulfur electrode, nonmetallic properties of sulfur and electrochemical products, shuttle effect.

With the rapid development of science and technology and the continuous improvement of people's demand, there are many research bottlenecks and opportunities. In the research field of new energy vehicles, the most promising lithium ion battery and hydrogen fuel cell also have many problems that need to be solved. In this paper, porous carbon substrates were prepared from sodium lignosulfonate and two popular electrode modifiers were combined to study the electrochemical properties of lignin carbon nanocomposites.

2. EXPERIMENTAL SECTION

2.1 Synthesis mechanism of lignin microspheres

Sodium lignosulfonate is soluble in water, but not in isopropyl alcohol. Tween-80 is soluble in alcohol and is generally used as an emulsifier for inverse emulsion polymerization in polymers.

Therefore, isopropyl alcohol can be used as a dispersing medium, and sodium lignosulfonate dissolved in water can be evenly dispersed in isopropyl alcohol by ultrasonic method. Due to the large molecular weight of sodium lignosulfonate itself, the combined microspheres are more likely to form many pores. So the post-treated lignin microspheres are burned at high temperature to evaporate the attachments on the carbon shelf, and stable porous carbon spheres should be obtained. Sodium lignosulfonate obtained under different conditions are different. In order to ensure that the raw materials used in this experiment can effectively synthesize lignin carbon spheres, the infrared spectrum scanning test was carried out. It was found that there was a strong wide peak at about 3432 cm^{-1}, indicating a large number of phenolic hydroxyl groups. There is a weak narrow peak at about 1650 cm^{-1} due to the vibration of the carbon-carbon double bond of the benzene ring in sodium lignosulfonate. There was a strong peak at 1250 cm^{-1}, indicating that sodium lignosulfonate had a large number of active reactive groups such as sulfonic group and hydroxyl group. The existence of these active groups makes it easily soluble in water but difficult to disperse evenly in organic solvents such as ethanol. Therefore, the sodium lignosulfonate used in this experiment meets the conditions of one-step ultrasonic assembly in isopropanol. Lignosulfonate aqueous solution containing Twin-80 is dropped into isopropanol. With the action of these reaction groups and surfactants, the molecular chain of lignin will slowly retract and self-assemble into lignin microspheres.

2.2 Preparation of lignin-based C/S composites

Preparation of lignin carbon pellets. First, weigh 1.2g sodium lignosulfonate in a 50 mL beaker, add 40 mL deionized water and stir. Then, 20 drops of Tween-80 surfactant were added to the beaker with dropper and placed in the ultrasonic pool until there was no obvious granular precipitation at the bottom, and lignin dispersion was obtained. Next, a 500 mL round-bottomed flask was filled with 500 mL isopropyl alcohol and placed in an ultrasound tank for ultrasound and agitation. Then, 20 mL lignin dispersion was injected into the flask at a rate of 20 $mL \cdot h^{-1}$ using a two-channel injection pump. After the injection, ultrasound was performed for 2 h. After the ultrasound, the mixture was centrifuged at a speed of 6000 $r \cdot min^{-1}$, and the centrifuged precipitates were dried in a vacuum oven for more than 24 h. After thorough drying, the brown-yellow solid was obtained, which was ground into powder with a mortar and put into a tubular furnace for carbonization and calcining. Then the lignin carbon pellets were obtained, which was recorded as LC. Elemental sulfur load. 0.01 g lignin carbon ball and 0.025 g sublimated sulfur were mixed in a 50 mL high-pressure reaction kettle, and 2 mL carbon disulfide was added. Then supercritical carbon dioxide was injected into it and reacted for 5 hours at 120 ℃. After the reaction, carbon dioxide is slowly released and cooled to room temperature, resulting in the lignin carbon/sulfur mixture. Grind it into fine particles and dry it in vacuum.

2.3 Structure analysis and test characterization

The analysis and characterization methods used in the preparation of lignin-based C/S composites include scanning electron microscopy (SEM), transmission electron microscopy (TEM),

nitrogen adsorption (BET), X-ray diffraction (XRD), Fourier transform infrared spectroscopy (FT-IR), Raman spectroscopy, etc. The scanning electron microscope used in this experiment is S-4700 produced by Hitachi (Japanese). The acceleration voltage is 10 kV and the working distance is 8 mm. SEM is mainly used to confirm the morphology of material surface or section. The sample preparation method is as follows: take a trace of powdery material and add it to ethanol, and mix it evenly under the ultrasonic of CNC ultrasonic cleaner, then take a drop of it on the aluminum sheet with dropper, and spray gold in vacuum for 40 seconds after drying. The transmission electron microscope (TEM) is the JEM-100CXII produced by Japan Electronics Co. Ltd, with a maximum resolution of 0.14 mm, an acceleration voltage of 300 kV and an X-ray energy dispersion spectrometer (EDS). TEM can observe the internal morphology of the material, and distinguish the distribution and thickness of different atomic number components in the material according to the contrast. EDS can be used to analyze element content. The sample preparation method is as follows: take a trace of powdery material and add it into ethanol, mix it evenly under ultrasound, take a drop and dry it on a special copper net. The nitrogen adsorption device used is Micromeritics ASAP2020. BET test is mainly used to study the specific surface area and adsorption capacity of porous materials. By judging the type of BET test curve, the type and pore size of material surface can be roughly obtained. The method using put in 0.1g powder material, vacuum at 120℃, and then test under liquid nitrogen. The instrument used is a combined multifunctional X-ray diffraction analyzer of Neki Ultima V, Japan. XRD is mainly used to confirm the crystal structure of materials, and the instrument scan range is 5° to 80°. A sufficient amount of powdery material is placed and flattened on a glass plate, and then placed directly into the instrument for testing. The infrared spectrometer used was Thermo Fisher Nicolet 6700 from the United States, with a test range of 500 cm^{-1} to 4000 cm^{-1}, resolution of 0.4 cm^{-1} and scanning frequency of 64. FTIR is mainly used to detect the molecular structure of chemical composition of materials. The sample preparation base is KBr. The material and KBr are ground and mixed evenly, and the tablet is pressed. Then the sample can be put into the instrument for testing. The instrument used was Thermo Fisher DXR, with a wavelength of 532 nm and a power of 5 Mw. Raman spectroscopy is sensitive to the vibration of molecules in the carbon material, so it is used to analyze the structure of the carbon material in this experiment. The instrument used was Lab RAM HR UV800 laser Raman spectrometer from JOBIN YVON Company, France. The excitation light source wavelength was 325 nm, and the scanning range was 200 cm^{-1} to 3000 cm^{-1}. A small amount of carbon pellet powder can be directly tested on a slide.

2.4 Electrochemical performance test

For lignin-based C/S composite materials, electrodes were prepared first, PVDF and NMP were mixed evenly according to the mass of 1:20, stirred and dissolved at 60℃, and then put into the oven. Remove from the oven every 15 minutes and stir until the solution is transparent and viscous with no obvious particles. Then mix PVDF/NMP mixture, acetylene black and the material to be tested according to the mass ratio of 1:1:8. Then, the obtained slurry was evenly smeared onto copper foil with a diameter of 12 mm with a glass rod and placed in a vacuum oven to dry at 60 ℃. The dried copper sheet is pressed flat with a tablet press at 16 MPa. Finally, the copper sheet was baked in a vacuum oven for 12 h to

prepare the electrode sheet. Then the battery assembly was carried out. The CR2035 button battery assembly was used in this experiment. The whole assembly process was carried out in a glove box filled with argon gas. The process is as follows: (1) the electrode sheet, diaphragm, lithium metal sheet and gasket are placed on the positive electrode shell of the battery successively. (2) Adding a drop of electrolyte. (3) Sealing machine sealing battery. The charge-discharge performance of the assembled button battery was tested at a constant current density of 0.1 $mA \cdot g^{-1}$ at room temperature. Cyclic Voltammetry controls voltage changes within a certain range, scans with triangular waveform over time, and records current-potential curves, which can be used to analyze the reaction potential, reaction mechanism and kinetic characteristics of batteries during charge and discharge. The scanning rate is 0.1 $mV \cdot s^{-1}$ and the scanning voltage range is 0 V to 3 V. Electrochemical impedance spectroscopy (EIS) is used to collect the impedance data of the battery in equilibrium state and to study the internal conductivity of the battery. The test frequency range was 0.1 Hz to 100 kHz, the voltage amplitude was 5 mV, and the ambient temperature was room temperature.

For lignin-based C/S composites, electrodes and electrolytic cells were prepared first. Nafion was mixed with ethanol at a volume ratio of 1∶9, and 1 mL was mixed with an appropriate amount of carbon spheres to form slurry uniformly by ultrasound. The paste is evenly coated on carbon paper (1×1 cm^2), each coating makes carbon paper absorb clean and dry before the next coating, and finally makes carbon paper completely absorb 1 mL of slurry to be used as electrode. With the material electrode working electrode, Ag/AgCl electrode reference electrode, graphite electrode counter electrode, a three-electrode battery system was built to test the electrical properties of the material. The electrolyte was KOH solution with a concentration of 6M, and the voltage range was 0.2V to 0.6V. Linear sweep voltammetry is a common electrochemical method. It mainly controls the scanning voltage change, increases gradually with time, and records the potential current curve. The voltage corresponding to a current of 10 mA is set as the overpotential.

Cyclic voltammetry is mainly controls the scanning voltage change, carries on the triangle waveform scanning with the time and records the potential current curve. The type of REDOX reaction on the electrode can be obtained from the potential of the REDOX peak. The scanning rate is 0.1 $mV \cdot s^{-1}$ and the scanning voltage range is 0 V to 3 V.

3. RESULTS AND DISCUSSION

In order to explore the actual structure of the composites, XRD and Raman spectroscopy were used to analyze the composites as shown in Figure 1(a). The figure shows that the sample has an obvious peak near 2θ=28°, which is the characteristic peak of S8, indicating that the sulfur enters into the micropores of lignin carbon by the method of supercritical carbon dioxide loading, while part of the sulfur still retains its original structural characteristics in this process. The sample showed a sharp peak near 2θ=44°, corresponding to the characteristic diffraction peak of (100) crystal surface of graphite carbon, indicating that the lignin microspheres were successfully carbonized at high temperature, and the sample surface showed a certain graphitization structure [15]. After high temperature burning, the

organic carbon frame will not only evaporate the excess material in the hole, but also may have regular rearrangement of carbon. The rearrangement of the graphite structure is theoretically very conducive to electron conduction, which can make up for the defects caused by the insulation of sulfur and solid compounds of sulfur in lithium sulfur batteries.

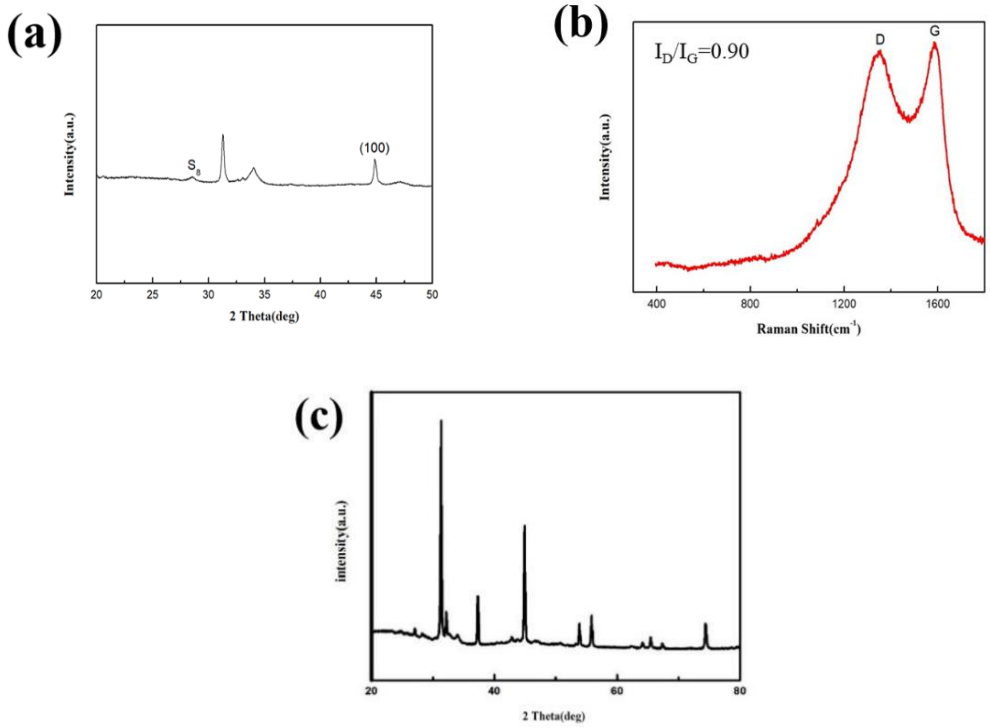

Figure 1. (a) XRD, (b) Raman spectrum of the Lignin-derived C/S microspheres and (c) XRD of the Lignin-derived Carbon microspheres

Figure 1 (c) shows the XRD patterns of lignin carbon microspheres for comparison. It can be seen that the three most prominent peaks including graphite (100) crystal face are corresponding in figure 1(a), while only one S8 characteristic peak is added in figure a), indicating that the method of loading sulfur with supercritical carbon dioxide does not damage the crystal structure of the original carbon spheres. The Raman spectra further characterize the graphitization degree of the composite microspheres in Figure 1 (b). The D peak at 1350 cm^{-1} represents the disordered carbon frame and material defects of the lignin microspheres, while the G peak at 1580 cm^{-1} represents the graphitized carbon after burning. The value of ID/IG in the calculated figure is 0.9, indicating that the graphitization degree of the material is relatively high, but there are still some defects. The defects include microcrystalline cavity structures, entanglement amorphous structures and lamellar edges, which also provide sites for electrochemically active reactions.

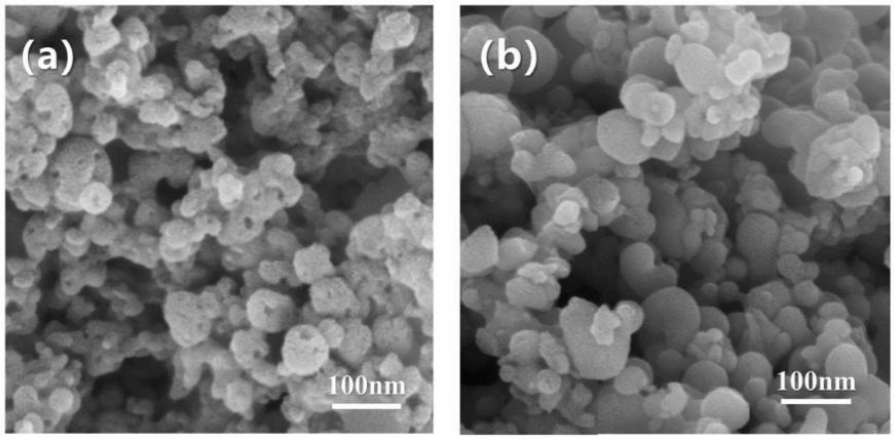

Figure 2. SEM microstructure images: (a) lignin-derived carbon microspheres, (b) lignin-derived C/S microspheres

In order to investigate the morphology changes of lignin carbon spheres loaded with sulfur, SEM was used to characterize the microstructure. Figure 2 (a) is the SEM diagram of lignin-based carbon spheres. As shown in the figure, the lignin-based carbon frames self-assembled in isopropanol form spherical particles of less than 100 nm with different diameters. Which is may caused by the wide molecular weight distribution of lignin itself.

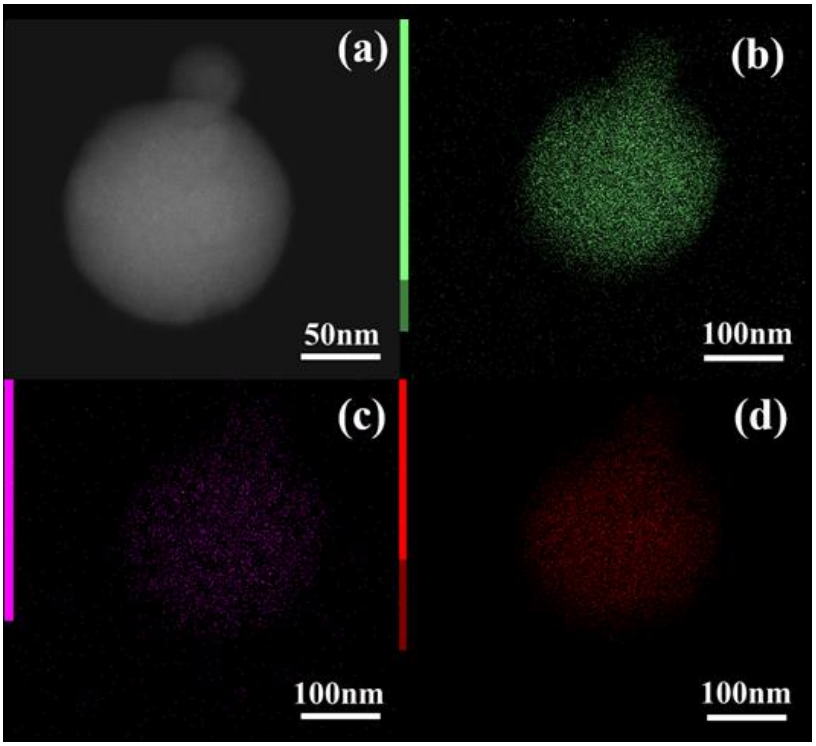

Figure 3. TEM and EDS images of the lignin-derived carbon microsphere

The surface of the microspheres is rough, and many pores can be clearly seen. These pores can absorb sulfur and sulfide to weaken the "shuttle effect", and also provide extra space for the sulfur combination reaction to weaken the volume strain of the electrode and improve the stability of the battery. Figure 2 (b) is obtained by supercritical carbon dioxide sulfur load of lignin base carbon/sulfur microspheres SEM figure. The surface of the microspheres is rough, and many pores can be clearly seen. These pores can absorb sulfur and sulfide to weaken the shuttle effect, and also provide extra space for the sulfur combination reaction to weaken the volume strain of the electrode and improve the stability of the battery.

In order to observe the specific morphology of the composite microspheres, the single microspheres were characterized by high resolution transmission electron microscopy. Figure 3 (a) shows two microspheres. It can be seen that the diameter difference between the two spheres is about 3 times, which is consistent with the observation result of SEM. The surface of the large ball is basically smooth and well-proportioned, with only two slight depressions visible and no large pores observed.

The EDS function attached with transmission electron microscope was used to test the microspheres to see the loading of sulfur as shown in Figure 3 (b-d), which is the distribution signal diagram of C, O and S elements of the two microspheres respectively. As can be seen from figures 3(b) and (c), the distribution of O on microspheres is fairly uniform due to the presence of many oxygen-containing groups in the C-skeleton of sodium lignosulfonate. The distribution of element S as shown in figure 3(d) is also particularly uniform, and even denser than the signal points of element O. It is known from the TEM diagram that there is no irregular sulfur agglomeration on the surface of the two microspheres, so this phenomenon can indicate that sulfur is uniformly loaded in the lignin carbon spheres under the action of supercritical carbon dioxide.

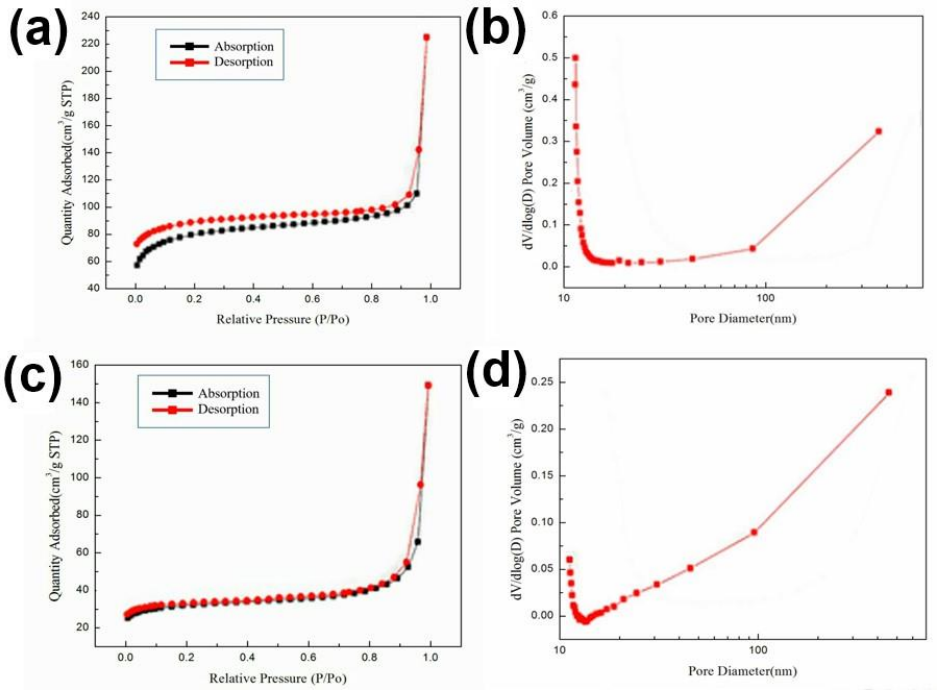

Figure 4. Specific surface area and pore size distribution (a,b) lignin-derived C microspheres and (c,d) lignin-derived C/S microspheres

BET is one of the most direct methods to detect the surface structure of materials. Figure 5 (a) and (c) are N_2 adsorption-desorption curves of original lignin-based carbon spheres and C/S composite microspheres, both of which have hysteresis phenomenon during desorption. The difference is that the curve in figure 4(a) did not close even in the low-pressure region, suggesting that the internal pores of the original carbon sphere collapsed, so that part of nitrogen was trapped inside the microsphere and could not be timely desorbed. Figure 4(c) is a typical type IV physical adsorption isotherm, which is closed at about 0.8 P/P0, forming a Type H3 hysteresis ring, indicating that it has large or a large number of interconnected holes. The specific surface area of the original carbon sphere was 259.8 $m^2 \cdot g^{-1}$, and the pore size was mainly over 30 nm except for a large number of micropores less than 1.5 nm. The composite microspheres was 39.95 $m^2 \cdot g^{-1}$. Compared with the original carbon spheres, the number of pores in the composite microspheres was reduced, but the number of micropores was significantly decreased. These results indicate that supercritical carbon dioxide can make sublimated sulfur uniformly cover the micropores on the surface of rough carbon spheres, which is consistent with the smooth morphology of carbon spheres under electron microscopy.

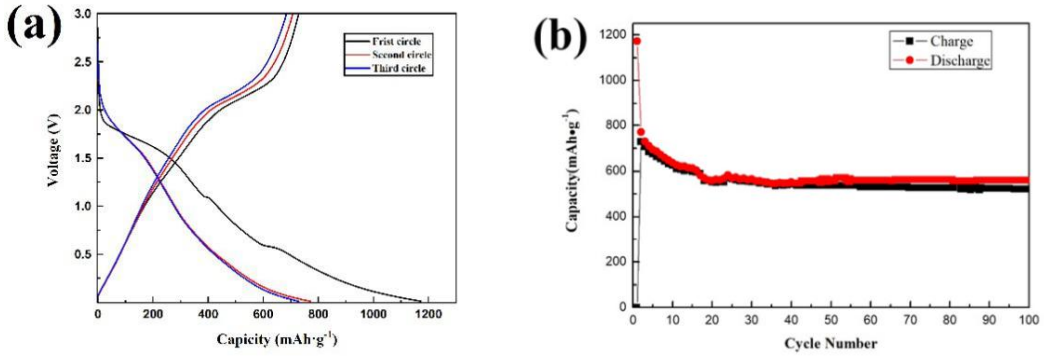

Figure 5. The constant current charge and discharge curve (a) and cycling performance of the lignin-derived C/S microspheres electrode (b)

Figure 5(a) shows the constant-current charge-discharge curves of the first three cycles of lignin-based C/S composite battery at 0.1 $mA \cdot g^{-1}$ current density, and the scanning voltage range is 0-3V. It can be seen that the battery has a first-ring discharge capacity of 1172 $mAh \cdot g^{-1}$, a charging capacity of 728 $mAh \cdot g^{-1}$, and a first-ring Coulomb efficiency of 62.1%. The discharge capacity of the second and third cycles decreased to 771 $mAh \cdot g^{-1}$ and 729 $mAh \cdot g^{-1}$, while the charging capacity decreased by 21.5 $mAh \cdot g^{-1}$ and 707 $mAh \cdot g^{-1}$ and 685 $mAh \cdot g^{-1}$, respectively. The reasons for capacity loss may include the following aspects: (1) The solid electrolyte interface film (SEI film, which is generally formed below 1.0V) is formed in the first discharge of lithium battery, and the electrode active substances are consumed [16]. (2) The sulfur in the microspheres is converted into soluble polysulfide (Li_2S_x, $4 \leq x \leq 8$, When discharging, such reaction occurs in the high voltage region), and permanently detach from the positive

electrode due to 'shuttle effect'. (3) High density solid polysulfide (Li_2S_x, $x \leq 2$, When discharging, this kind of reaction occurs in the low voltage region) and the resulting volumetric strain makes part of sulfur desorption. (4) Some S8 aggregates adsorbed on the surface of the microspheres provided capacity for initial discharge, but desorption did not take long. However, the obvious discharge reaction curve appeared from 1.9V in the first discharge, which should indicate that the initial discharge reaction of sulfur concentrated in the low voltage region of solid polysulfide formation. The tiny platform at 0.6V should represent the formation of SEI film. The shape of the discharge curves of the second and third cycles does not change much, which reflects the reversibility of the material reaction and proves that it can be reused, but there is no obvious platform. Similar oxidation platforms begin to appear at about 2.2 V in all three charging curves, which should correspond to the curing process of long-chain or partial short-chain polysulfide.

In order to further verify the cycle stability of lignin-based C/S composite battery, its cycle performance was tested at 0.1 $mA \cdot g^{-1}$ current density, as shown in Figure 5(b), the first 100 charge and discharge cycle curves of the battery. Except for the first cycle, the coulombic efficiency of the composite battery is more than 97%, and it retains 570 mAh·V capacity after 100 cycles, showing a excellent cycle stability.

The specific capacity of carbon composites were compared in table 1.

Table 1. The specific capacity of some common cathode materials

Cathode materials	Overpotential (V)
This work	0.306
Pure bamboo carbon [17]	0.431
Lignin carbon fibre [18]	0.442
VA-NCNT[19]	0.302
NOMGAs[20]	0.317
C-PDDA[21]	0.358
Traditional petroleum carbon	0.514

It can be seen from Table 1 that the traditional carbon material has a high over-potential, while the other carbon matrix composites have a relatively low over-potential. Transition metals and their oxides can provide low chemical sites and significantly reduce the overpotential of composites, which provides a new idea for the improvement of hydrogen evolution electrode. The porosity of carbon materials is also one of the hot topics for further research and development in the future.

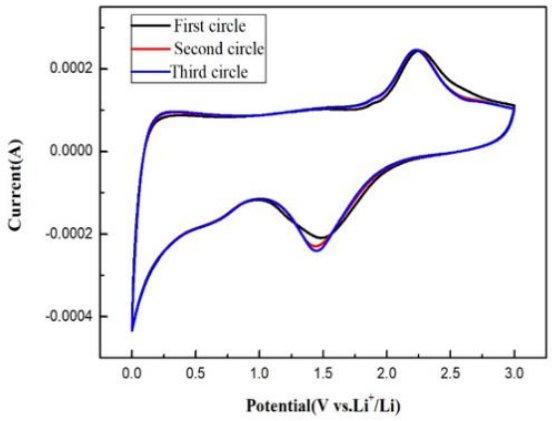

Figure 6. CV curves of C/S microspheres electrode

Figure 6 shows the 3-cycle voltammetry curve of lignin-based C/S composite battery at the scanning speed of 0.1 $mV \cdot s^{-1}$. There is a reduction peak at about 1.5 V in all three cycles, which corresponds to the reduction of sulfur or soluble polysulfide to low price solid polysulfide. There is no other obvious reduction peak, confirming the suspicion that the sulfur discharge reaction in the composite battery is concentrated in the formation of solid polysulfide. The oxidation peak appeared at about 2.2V, corresponding to the platform of the first three charging curves, representing the re-oxidation of polysulfide into sulfur elements. The high coincidence degree of the three cycle curves indicates the high reversibility of the REDOX reaction of the battery.

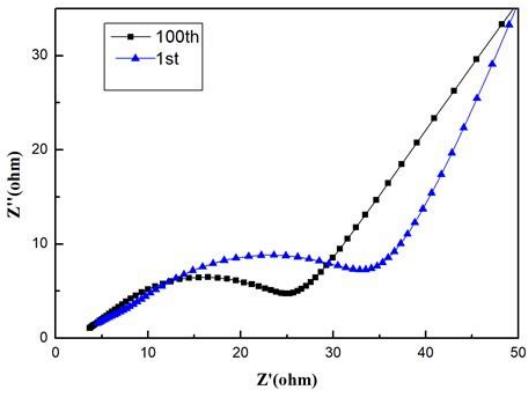

Figure 7. Nyquist plots of the lignin-derived C/S microspheres electrode

In order to study the change of the conductivity of lignin-based C/S composite battery, the electrochemical impedance of the lignin-based C/S composite battery was measured at the beginning and after 100 charge and discharge cycles, and represented by McQuist spectrum, as shown in Figure 7. The spectrum consists of a semicircle and a straight line, which represent the high frequency region and

the low frequency region respectively. Generally speaking, the semi-arc in the high frequency region represents the electrochemical resistance of the battery electrode material. The larger the diameter corresponding to the semi-circle is, the slower the charge transfer rate of the electrode is. The straight line in the low-frequency region corresponds to the electrochemical active unit of diffusion, and the smaller the slope of the line is, the slower the unit diffusion rate is [22]. It can be seen from the figure that after 100 charge and discharge cycles of the composite battery, the electrochemical impedance of the electrode decreases, while the diffusion impedance of the active unit increases slightly. According to the test and analysis, this could be as the charge and discharge cycle, the reunion of lignin base carbon ball surface adsorption of sulfur and sulfur gradually stripping, plugging the pores of the carbon ball in the hole and the hole can allow insulation Li_2S_2 solid state to some extent the formation of Li_2S and this makes lignin Quito hole carbon conductive role to play. However, some solid Li_2S_2 and Li_2S generated in the concentrated battery reaction fall off in the electrolyte or grow outside the lithium electrode due to ‘shuttle effect’, which hinders the diffusion of lithium ions [23].

4. CONCLUSIONS

Lignin-based porous carbon spheres were prepared by one-step ultrasonic self-assembly and high-temperature calcination, and the C/S composite microspheres were formed by loading sulfur with supercritical carbon dioxide method. The morphology and structure tests show that the microspheres prepared in this experiment contain many microholes and have a high degree of graphitization. The sulfur is uniformly loaded on the microspheres, which can be used for electrochemical testing. Then, the lignin-based C/S composite electrode was prepared and electrochemical test was carried out. The results showed that the initial discharge capacity of the lignin-based C/S composite electrode reached 1172 $mAh \cdot g^{-1}$ at the current density of 0.1 $mA \cdot g^{-1}$, and the capacity retained at 570 $mAh \cdot g^{-1}$ after 1100 charge and discharge cycles, and the capacity retention rate was 48.6%. A cyclocoulomb efficiency of more than 97%, which reached the normal level of the porous carbon-sulfur composite electrode.

References

1. L. Du, X.M. Yan, G.H. He, X.M. Wu, Z.W. Hu and Y.D. Wang, *Int. J. Hydrogen Energ.* 37 (2012) 11853.
2. V. Malgras, Q. Ji, Y. Kamachi. *Bull. Chem. Soc. Jpn.*, 88 (2015) 1171.
3. B. Guo, X. Wang, P.F. Fulvio. *Adv. Mater.*, 23 (2011) 4661.
4. Z. Liu, J. Li, S. Xue. *J. Energy Chem.*,47 (2020) 317.
5. L. Sterk, J. Gorka, A. Vinu. *Microporous Mesoporous Mater.*, 156 (2012) 121.
6. H. Wang, S. Min, C. Ma. *Nat. Commun.*, 8 (2017) 13592.
7. J. Deng, T. Xiong, F. Xu. *Green Chem.*, 17 (2015) 4053.
8. V.D.P. Daniel, H. Aynsley, D. Lloyd. *BioResourses*, 6 (2011) 1105.
9. M. Yang, J. Zhang, W. Zhang. *J. Alloys Compd.*, 823 (2020) 153790.
10. D.M.F. Santos, C.A.C. Sequeira, D. Maccio. *Int. J. Hydrog. Energy*, 38 (2013) 3137.

11. H.C. Liu, A.T. Chien, B.A. Newcomb. *ACS Sustain. Chem. Eng.*, 3 (2015) 1943.
12. S. Imtiaz, J. Zhang, Z.A. Zafar. *Sci. China Mater.*, 59 (2016) 389.
13. X. Liang, C.Y. Kwok, F. Lodi-Marzano. *Adv. Energy Mater.*, 6 (2016) 1501636.
14. T. Schaffer, T. Tschinder, V. Hacker and J.O. Besenhard, *J. Power Sources*, 153 (2006) 210.
15. S.Y. Jiang, X. Yu, L.T. Han, D. Qiao, Z.P. Zhao, J.H. Wang. *J Electrochem Sci*, 16(2021) 211014
16. J.J. Hwang. *Renew. Sust. Energ. Rev.*, 16 (2012) 3803.
17. Z.P. Zhao, Z.P. Zhou and M. Q. Zhong. *Int. J. Electrochem. Sci.*, 12 (2014) 8120.
18. M. M. Ren, M. Z. Yang, W. L. Liu, M. Li and H. Y. Ma, *Electrochim. Acta*, 194 (2016) 219.
19. J. Fu, Y. Huang, Y. Pan, Y. Zhu, X. Huang and X. Tang. *Mater. Lett.*, 62 (2008) 4130.
20. C. Li, M. Zhao, C. N. Sun, B. Jin, C. C. Yang and Q. Jiang, *J. Power Sources*, 397 (2018) 162.
21. C. Hu and L. Dai. *Adv. Mater.*, 29 (2017) 1604942.
22. Z. Liu, J. Li, S. Xue. *J. Energy Chem.*,47 (2020) 317.
23. M. Yang, J. Zhang, W. Zhang. *J. Alloys Compd.*, 823 (2020) 153790.